Aalto University

Aaltodoc
OPEN ACCESS

This is an electronic reprint of the original article.
This reprint may differ from the original in pagination and typographic detail.

Author(s): Olsson, Anders & Aierken, Abuduwayiti & Jussila, Henri & Bauer, Jan & Oksanen, Jani & Breitenstein, Otwin & Lipsanen, Harri & Tulkki, Jukka

Title: Yield and leakage currents of large area lattice matched InP/InGaAs heterostructures

Year: 2014

Version: Final published version

Please cite the original version:

Olsson, Anders & Aierken, Abuduwayiti & Jussila, Henri & Bauer, Jan & Oksanen, Jani & Breitenstein, Otwin & Lipsanen, Harri & Tulkki, Jukka. 2014. Yield and leakage currents of large area lattice matched InP/InGaAs heterostructures. Journal of Applied Physics. Volume 116, Issue 8. P. 083105/1-6. ISSN 0021-8979 (printed). DOI: 10.1063/1.4894005.

Rights: © 2014 American Institute of Physics. This article may be downloaded for personal use only. Any other use requires prior permission of the author and the American Institute of Physics. http://scitation.aip.org/content/aip/journal/jap

All material supplied via Aaltodoc is protected by copyright and other intellectual property rights, and duplication or sale of all or part of any of the repository collections is not permitted, except that material may be duplicated by you for your research use or educational purposes in electronic or print form. You must obtain permission for any other use. Electronic or print copies may not be offered, whether for sale or otherwise to anyone who is not an authorised user.

AIP | Journal of Applied Physics

Yield and leakage currents of large area lattice matched InP/InGaAs heterostructures

Anders Olsson, Abuduwayiti Aierken, Henri Jussila, Jan Bauer, Jani Oksanen, Otwin Breitenstein, Harri Lipsanen, and Jukka Tulkki

Citation: Journal of Applied Physics **116**, 083105 (2014); doi: 10.1063/1.4894005
View online: http://dx.doi.org/10.1063/1.4894005
View Table of Contents: http://scitation.aip.org/content/aip/journal/jap/116/8?ver=pdfcov
Published by the AIP Publishing

Articles you may be interested in
Ultrathin InAlN/GaN heterostructures on sapphire for high on/off current ratio high electron mobility transistors
J. Appl. Phys. **113**, 214503 (2013); 10.1063/1.4808260

InP-based 2.8–3.5 μm resonant-cavity light emitting diodes based on type-II transitions in GaInAs/GaAsSb heterostructures
Appl. Phys. Lett. **101**, 221107 (2012); 10.1063/1.4768447

Charge storage properties of InP quantum dots in GaAs metal-oxide-semiconductor based nonvolatile flash memory devices
Appl. Phys. Lett. **101**, 212108 (2012); 10.1063/1.4767522

Growth and characterization of iron-doped semi-insulating InP buffer layers for Al-free GaInP/GaInAs high electron mobility transistors
J. Appl. Phys. **108**, 114502 (2010); 10.1063/1.3516490

InGaAs/InP double heterostructures on InP/Si templates fabricated by wafer bonding and hydrogen-induced exfoliation
Appl. Phys. Lett. **83**, 5413 (2003); 10.1063/1.1637429

MIT LINCOLN LABORATORY CAREERS

Discover the satisfaction of innovation and service to the nation

- Space Control
- Air & Missile Defense
- Communications Systems & Cyber Security
- Intelligence, Surveillance and Reconnaissance Systems
- Advanced Electronics
- Tactical Systems
- Homeland Protection
- Air Traffic Control

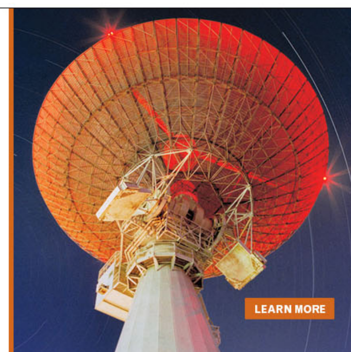

[This article is copyrighted as indicated in the article. Reuse of AIP content is subject to the terms at: http://scitation.aip.org/termsconditions. Downloaded to] IP: 130.233.216.27 On: Tue, 05 May 2015 09:07:47

JOURNAL OF APPLIED PHYSICS **116**, 083105 (2014)

Yield and leakage currents of large area lattice matched InP/InGaAs heterostructures

Anders Olsson,[1,2,a)] Abuduwayiti Aierken,[2] Henri Jussila,[2] Jan Bauer,[3] Jani Oksanen,[1] Otwin Breitenstein,[3] Harri Lipsanen,[2] and Jukka Tulkki[1]
[1]*Department of Biomedical Engineering and Computational Science, Aalto University, P.O. Box 12200, FI-00076, Finland*
[2]*Department of Micro- and Nanosciences, Micronova, Aalto University, P.O. Box 13500, FI-00076, Finland*
[3]*Max Planck Institute of Microstructure Physics, Weinberg 2, 06120 Halle, Germany*

(Received 3 July 2014; accepted 14 August 2014; published online 26 August 2014)

Demonstrating and harnessing electroluminescent cooling at technologically viable cooling powers requires the ability to routinely fabricate large area high quality light-emitting diodes (LEDs). Detailed information on the performance and yield of relevant large area devices is not available, however. Here, we report extensive information on the yield and related large area scaling of InP/InGaAs LEDs and discuss the origin of the failure mechanisms based on lock-in thermographic imaging. The studied LEDs were fabricated as mesa structures of various sizes on epistructures grown at five different facilities specialized in the growth of III-V compound semiconductors. While the smaller mesas generally showed relatively good electrical characteristics and low leakage current densities, some of them also exhibited unusually large leakage current densities. The provided information is critical for the development and design of the optical cooling technologies relying on large area devices. © *2014 AIP Publishing LLC*. [http://dx.doi.org/10.1063/1.4894005]

I. INTRODUCTION

Light emitting diodes (LEDs) based on the conventional III-V compound semiconductor double heterojunctions (DHJ) and GaAs/GaInP DHJs in particular are known to exhibit internal quantum efficiencies (IQE) that are very close to unity.[1–3] Ideally, the high IQE is expected to enable electroluminescent (EL) cooling[4,5] if the high IQE can be converted to a high external quantum efficiency (EQE) by very efficient light extraction or by adopting thermophotonic (TPX) approaches where the light is absorbed within the semiconductor material.[6] While EL cooling at technologically relevant power levels is yet to be demonstrated, the expectations for functional thermophotonic coolers have very recently been reinforced by the progress and first demonstrations of optical refrigeration in doped glasses[7,8] and II-IV compound semiconductors[9] as well as the demonstrations of very low power EL cooling in GaSb/InGaAsSb LEDs.[10,11] Although the first EL cooling demonstrations took place under very low bias voltages, they demonstrated electricity-to-light conversion efficiencies exceeding unity by a large margin. However, to increase the cooling power, optimized large area LED structures are needed.

InP and InGaAs based material systems rise as natural candidates for studying and realizing TPX devices, since they represent mature technologies that enable fabricating high quality lattice matched DHJ structures. While record-high IQEs have been reported for devices fabricated on GaAs,[2] fabricating efficient LEDs typically requires lifting off[12,13] the GaAs substrate. On the other hand, the InGaAsP material system readily allows the fabrication of a thick lattice matched DHJ structure on a transparent InP substrate. These material systems have also been reported to enable large area (up to several cm^2), high efficiency devices, particularly in the form of GaAs, InP, and InP/InGaAs[14–17] solar cells, but there are very few reports on the detailed performance, yield, and scalability of these devices, especially in the DHJ LED configuration.

In this report, we systematically study the electrical performance, yield, and distribution of reverse currents of standard InP/InGaAs LEDs processed on epistructures fabricated at five different locations. This includes analyzing the current density-voltage (J-V) behavior of hundreds of LEDs to obtain statistics of their leakage currents and lock-in thermography imaging of the samples to study heating associated with the current distributions in the LEDs. This information is essential in developing and designing LEDs suitable for future EL cooling devices where large area LEDs can enable increasing the cooling power and low leakage current is an essential prerequisite for enabling the high efficiency required to reach the EL cooling regime.

II. EXPERIMENT

A. Samples

The epitaxial structures A-E used to fabricate the LEDs were obtained from five different facilities. As shown in Fig. 1, the active region (AR) in all the structures consists of an unintentionally doped 300 nm InGaAs layer lattice matched to InP and surrounded by thin unintentionally doped InP barrier layers and the p- and n-type layers. Structures A, C, and D were grown by university affiliated groups and structures B and E were grown at commercial facilities. The structures grown at our own university were fabricated using a horizontal metalorganic vapor phase epitaxy (MOVPE) reactor at

[a)]Electronic mail: anders.olsson@aalto.fi

 © 2014 AIP Publishing LLC

[This article is copyrighted as indicated in the article. Reuse of AIP content is subject to the terms at: http://scitation.aip.org/termsconditions. Downloaded to] IP: 130.233.216.27 On: Tue, 05 May 2015 09:07:47

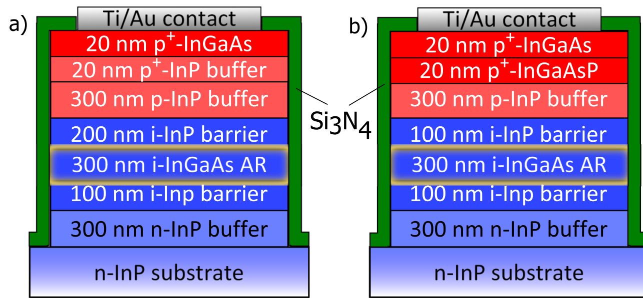

FIG. 1. The studied LED structures were fabricated as square mesas on epitaxial structures grown at several facilities. The structures were grown on n-type double side polished substrates and the essential features of samples (a) A–D and (b) E are identical except for the small differences in the p-contact layers and the i-InP barrier thickness on top of the AR.

atmospheric pressure. In this case, the precursors used for In, Ga, As, and P where trimethylindium (TMIn), trimethylgallium (TMGa), tertiarybutylarsine (TBAs), and tertiarybutylphosphine (TBP), respectively, and the growth temperature was 650 °C.

Each of the structures were then processed to contain a large number of square shaped LED mesas, grouped by size, as detailed in Table I. The mesas were formed using standard selective wet etching techniques. First, a Si_3N_4 layer and photoresist layer were deposited on top of each structure A-E. Then the photoresist layer was patterned and the mesa structures were formed by selective etching, using BHF:H_2O (1:10, 1 min etching time), H_3PO_4:H_2O_2:H_2O (1:1:10, etching rate 80 nm/min), and H_3PO_4:HCl (6:1, etching rate 400 nm/min) for the Si_3N_4, InGaAs/InGaAsP, and InP layers, respectively. After this, the structures were again covered with Si_3N_4 and a resist patterned to enable square shaped openings on top of the mesas.

Ti/Au 50/300 nm metal layers were then evaporated on the structures and lifted-off to form p-contacts covering the entire mesa area except for a 30 μm strip from the mesa edges. Liquid InGa was used as the n-type contacts at the bottom of the substrates.

B. Ideal diode law and typical unidealities

The J-V relationship measured in all LED samples differs significantly from idealized LED models. To better highlight the differences, we first discuss the LED carrier recombination and basic unidealities. In general, the current density J_{id} of an ideal (no shunt currents) LED can be written as[18]

$$J_{id} = J_{rad} + J_{SRH} + J_{Auger} + J_{pn}, \tag{1}$$

where J_{rad}, J_{SRH}, and J_{Auger} are the current density components due to radiative, Shockley-Read-Hall (SRH), and Auger recombination or generation, respectively, and J_{pn} is the current density component due to current flow over the p-n junction.

The first three terms on the right hand side in Eq. (1) are generated by recombination current in the AR and can be approximated by the typical ABC recombination model as[18]

$$J_{rec} = J_{rad} + J_{SRH} + J_{Auger} = e\,d(An + Bn^2 + Cn^3), \tag{2}$$

where e is the elementary charge, d is the thickness of the AR or quantum well, A, B, and C are the Shockley-Read-Hall, radiative, and Auger recombination coefficients, respectively, and n is the density of excess electrons and holes. In addition to assuming equal electron and hole density, Eq. (2) also assumes that n is much larger than the intrinsic carrier density.

When the Boltzmann approximation holds and charge neutrality is assumed, the carrier density depends on the electrical excitation as $n = n_i\, e^{eU_a/(2kT)}$, where T is the temperature, k is the Boltzmann constant, U_a is the separation of the quasi-Fermi levels in the AR, and n_i is the intrinsic carrier density. In addition to the recombination current due to recombination in the AR, the current through the LED also includes a p-n diode component due to recombination and charge transfer in the barrier layers, given by the Shockley equation[19] $J_{pn} = J_s[e^{e(U_a)/(n_{ideal}kT)} - 1]$, where J_s is the material specific saturation current density and n_{ideal} is the ideality factor.

The voltage U and current density J over an unideal LED can then be parametrized using U_a as $U(U_a) = U_a + R_s A J(U_a)$ and $J(U_a) = J_{id}(U_a) + U_a/(R_p A)$, where R_s and R_p are the series and shunt resistances of the unideal LED, respectively, and A is the cross-sectional area. The effects of the parasitic resistances on the LED behavior are schematically shown in Fig. 2, showing that the main effects of a shunt resistance are a non-saturating reverse bias current

TABLE I. List of the LED structures studied in this work.

Mesa group	Fabrication method	LED identifiers	Area (μm^2)	Origin
A1	MOVPE	1–98	500 × 500	University
A2		1–2	4000 × 4000	
B1	MOVPE	1–98	500 × 500	Commercial
B2		1–2	4000 × 4000	
C1	MBE	1–98	500 × 500	University
C2		1–2	4000 × 4000	
D1	MOVPE	1–98	500 × 500	University
D1		1–2	4000 × 4000	
E1	MOVPE	1–98	500 × 500	Commercial
E2		1–2	4000 × 4000	
E3		1–50	200 × 200	
E4		1–16	1800 × 1800	

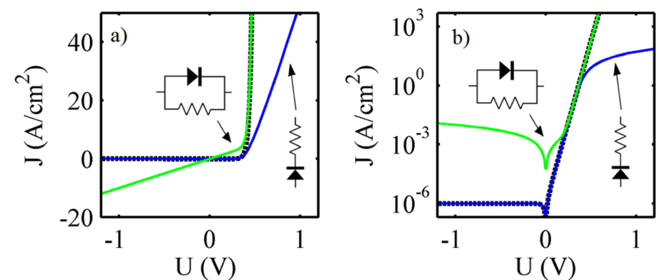

FIG. 2. The ideal diode current density (black dashed line) as a function of voltage on (a) linear and (b) logarithmic scale. The green and blue lines approximate the unideal performance commonly described by resistors in parallel or series with the ideal diode, as shown in the insets.)

[This article is copyrighted as indicated in the article. Reuse of AIP content is subject to the terms at: http://scitation.aip.org/termsconditions. Downloaded to] IP: 130.233.216.27 On: Tue, 05 May 2015 09:07:47

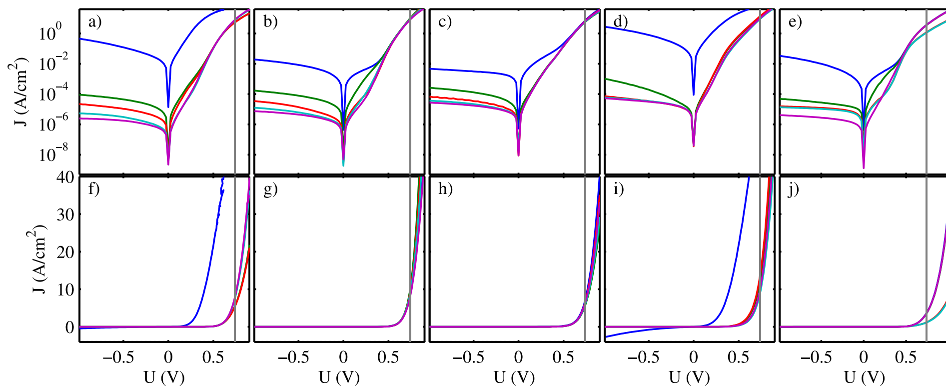

FIG. 3. The J-V measurements from samples A1-E1 in logarithmic (a)–(e) and linear (f)–(j) scale. The plotted curves have been chosen to represent samples with the smallest and largest leakage currents as well as three intermediate samples representing the median and the 25th and 75th percentiles. The gray line shows the threshold voltage at 0.74 V, which corresponds to the InGaAs band gap.

and a small shoulder in the forward current seen in the plot with logarithmic scale, while a series resistance strongly limits the exponential behavior under forward bias.

The reverse current density in an LED under moderate reverse biases $U \ll -kT/e$ is mainly determined by the shunt resistance caused by the unidealities and the generation rate of electron-hole pairs due to SRH-generation (i.e., the reverse process of the SRH recombination), and therefore gives a relatively good measure of the device quality. The commonly used linear shunt current model introduced above is useful for phenomenologically describing and quantifying the unidealities of an LED. Note however, that the dependence of the shunt currents on the voltage is generally not linear[20,21] in real devices.

III. RESULTS

We have performed J-V measurements on all devices listed in Table I using a four-point-probe to study device performance through statistical analysis. Fig. 3 shows the measured current density as a function of voltage from five mesas in each mesa group A1-E1. The plotted curves have been chosen to represent devices with the smallest and largest leakage currents as well as three intermediate devices representing the median and the 25th and 75th percentiles. In general, there is a difference of several orders of magnitude between the smallest and largest values of the leakage current at -1 V reverse bias. While the leakage current of the best performing mesas is only a few μA/cm^2 for each group of mesas A1-E1, the leakage current of the worst performing mesas varies considerably. This is expected to directly reflect the generally uniform quality of the material in the mesas in groups A1-E1: when there are no significant defects within the mesa, relatively small leakage currents are observed, but if the mesa happens to contain even an isolated defect allowing current leakage the leakage current increases by several orders of magnitude. The threshold voltages of the studied structures vary slightly, but are generally below 0.74 V which corresponds to the band gap ($E_g = 0.74$ eV) of lattice matched InGaAs shown by the gray vertical line in Fig. 3.

To get a better picture of how the leakage currents are distributed on the structures, Fig. 4 shows the distribution of the leakage currents of the mesas in groups A1-E1 at a bias of -1 V. In general, the reverse bias current density in most of the mesas lies within a relatively narrow regime below the value of a few hundred μA/cm^2 with a few outliers with several orders of magnitude larger current densities. The mesas in group D1 exhibit the largest leakage currents, including one count of over 1 A/cm^2.

To quantify the density of the defects leading to failed devices, we calculated the upper limit of the defect density as $(N_f + 1)/A$, where N_f is the number of devices where the reverse current at -1 V exceeds a failure current describing the limit between failed and functional devices and A is the area of the mesa. Fig. 5 shows the upper limit for the defect density and the corresponding failure percentage for the mesas in groups A1-E1. For the majority of the epitaxial structures, the defect density decreases relatively fast as the failure threshold increases, although structure D deviates from this behavior by exhibiting nearly an order of magnitude higher defect density than the rest of the structures. Apart from the mesas in group D1, the defect density is typically smaller than 10/cm^2 when reverse current densities of 10 mA/cm^2 are allowed.

Fig. 6 shows the J-V measurements of the 4×4 mm^2 mesas in groups A2-E2 as examples of larger device area structures. The typical leakage current densities are of the order of a few mA/cm^2, i.e., considerably larger than for the best 500×500 μm^2 mesas, except for structure E where the leakage current of one of the large area devices is quite small. The statistical variation due to the small number of samples is clearly visible, even between mesas on the same

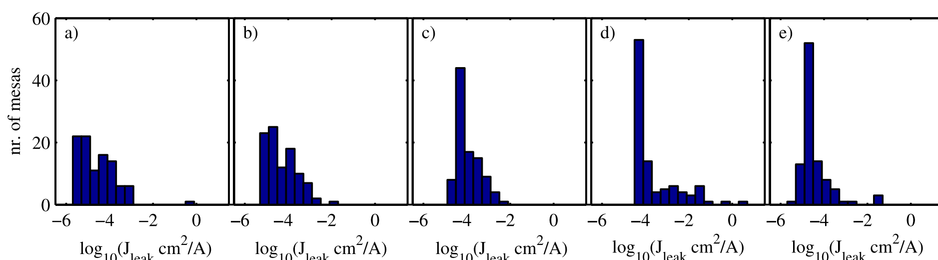

FIG. 4. The distribution of the leakage current densities at a bias of -1 V for the mesas in groups A1–E1. For the majority of the mesas, the current density lies below a few hundred μA/cm^2, but a few mesas also exhibit several orders of magnitude larger leakage current densities.

[This article is copyrighted as indicated in the article. Reuse of AIP content is subject to the terms at: http://scitation.aip.org/termsconditions. Downloaded to] IP: 130.233.216.27 On: Tue, 05 May 2015 09:07:47

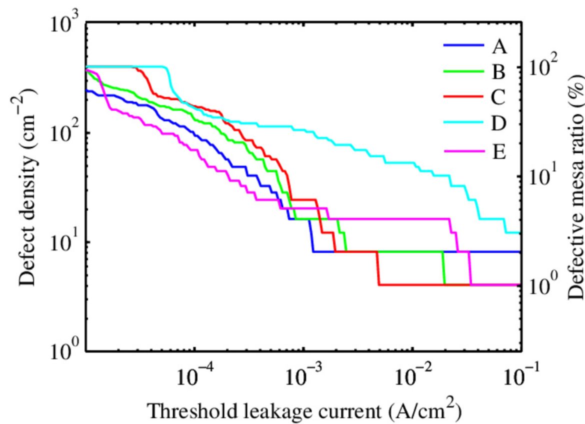

FIG. 5. Upper limit for the defect density in the epitaxial layers defined as a function of a failure current for mesas in groups A1–E1. The right axis shows the upper limit for the percentage of defective mesas on each epistructure. Discontinuities in the curves follow from discrete statistical data.

structures. The apparent decrease in the threshold voltage in linear scale compared to the measurements in Fig. 3 is mostly caused by the fact that the maximum current allowed in the measurement setup is 100 mA, which significantly decreases the maximum measurable current density for the larger area mesas.

To study how the leakage current scales with the mesa size, further measurements were performed on the mesas with side lengths between 200 and 4000 μm in groups E1-E4. Fig. 7 shows the leakage current of the least leaking mesas as a function of mesa area and mesa circumference in each group E1-E3. The measurement of group E4 was left out of the figure because of deviation caused by statistical uncertainty due to the small number of measured large area mesas. The leakage current scales approximately linearly with the mesa circumference. Assuming that the best performing mesa structures can be considered uniform, this suggests that the leakage current in the best structures is mainly caused by surface currents generated at the SiN_4 protected mesa edges.

To check the uniformity of the composition in the structures, photoluminescence (PL) spectra of the epistructures A-E were also studied. Fig. 8 shows the spectra measured on an equally spaced 5×5 grid of points on a $4 \times 4\,mm^2$ area on the surface of structure E. The shift in the peak wavelength of the PL spectra is negligible suggesting that the material composition is uniform. All spectra peak at approximately 1664 nm which closely corresponds to the expected band gap of lattice matched InGaAs. The structures were also studied by AFM and the results suggest a relatively uniform surface morphology. Generally, the surfaces were observed to show a roughness well below 10 nm but in some rare cases also pits at least several tens of nanometers deep and a few hundreds of nanometers wide were found.

In order to examine whether the leakage currents are affected by dislocations 008 back-reflection synchrotron x-ray diffraction (XRD), topography[22] measurements were taken from a large number of the samples. Fig. 9 shows topographs of mesa nr. 18 in mesa group D1 and mesa nr. 48 in mesa group E1 with the J-V curves of the mesas shown in the inset. Mesa D1#18 was chosen as an example of poor device quality in terms of crystal quality, while mesa E1#48 represents a standard device with only minor defects. In mesa D1#18 shown in Fig. 9(a) misfit dislocations, displayed as white vertical lines, cover most of the grown area. Additionally, the mesa exhibits crater looking dots with unknown origin. Mesa E1#48 shown in Fig. 9(b) shows a much smoother structure with hardly any defects. Despite the clearly inferior crystal quality of mesa D1#18, the J-V curves of the samples are not dramatically different, suggesting that dislocations or other irregularities visible in the topograph are not directly correlated with leakage currents in the corresponding mesas.

In order to gain further knowledge in pinpointing the locations of the leakage current paths in the LEDs, dark lock-in thermography (DLIT)[23] measurements were performed on selected samples A1-E1. To increase the emissivity of the otherwise very reflective gold contacts, the mesas were covered with non-conductive ink before the measurement. Generally, the heating of the LEDs under forward bias is distributed relatively evenly in the mesa area, with the largest changes caused by current crowding near the current injecting probe needle and temperature gradients due to changes in thermal conduction and dissipation near the edges. Under reverse bias, the signal is typically too weak to be seen and just noise is observed except for the mesas exhibiting the largest leakage currents. When the mesa does exhibit a relatively large leakage current, there is typically a single point-like heat signal on the mesa or at the mesa edge. An example of the forward current temperature distribution with $U = 0.6$ V and $I = 6$ mA is shown in Fig. 10(a). As usual, the largest increase in the temperature is observed in

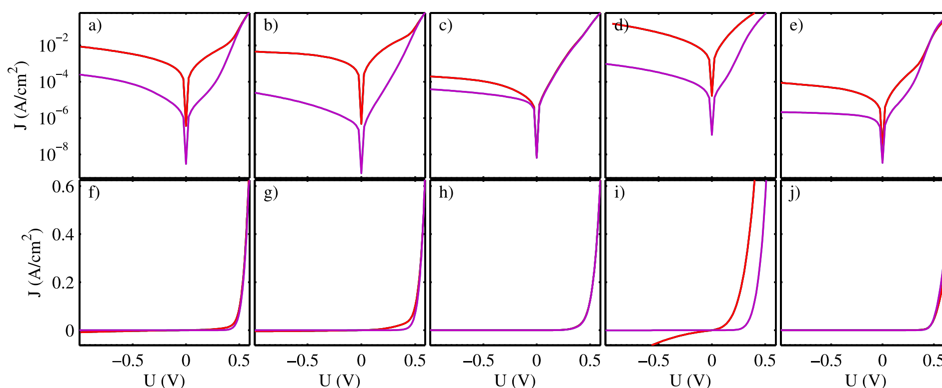

FIG. 6. J-V measurements from the mesas in groups A2-E2 in linear (a)–(e) and logarithmic (f)–(j) scale.

[This article is copyrighted as indicated in the article. Reuse of AIP content is subject to the terms at: http://scitation.aip.org/termsconditions. Downloaded to] IP: 130.233.216.27 On: Tue, 05 May 2015 09:07:47

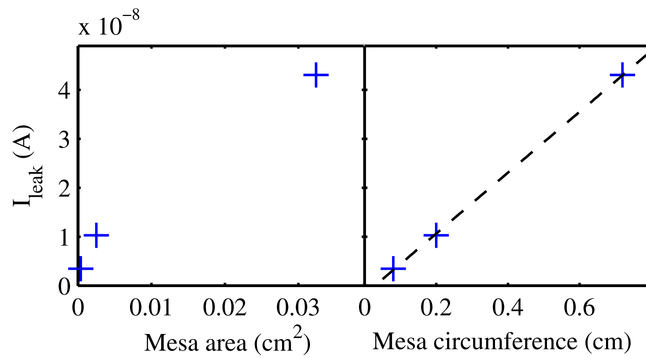

FIG. 7. The leakage current as a function of (a) mesa area and (b) as a function of circumference for the least leaking mesas in groups E1-E3, at a bias of −1 V. The dashed line shows a linear least squares fit to the data points in (b).

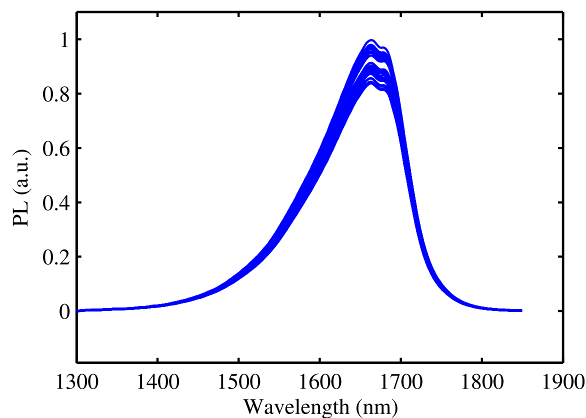

FIG. 8. PL spectra for epistructure E measured on an equally spaced 5 × 5 grid of points on a 4 × 4 mm area measured with an excitation density of 410 W/cm^2 using a 1064 nm pump laser with a beam diameter of 150 μm on the sample surface.

the center of the mesa and around the current injecting probe tip and to a lesser degree at the edges. Fig. 10(b) shows the temperature distribution on the same mesa, under reverse bias, at $U = -1$ V and $I \ll 1$ mA. In contrast to most other mesas, a clear heat signal from a single point a few tens of μm from the edge of the mesa is observed. Generally, the DLIT measurements indicate either point-like reverse leakage or no significant leakage current in the structures. This

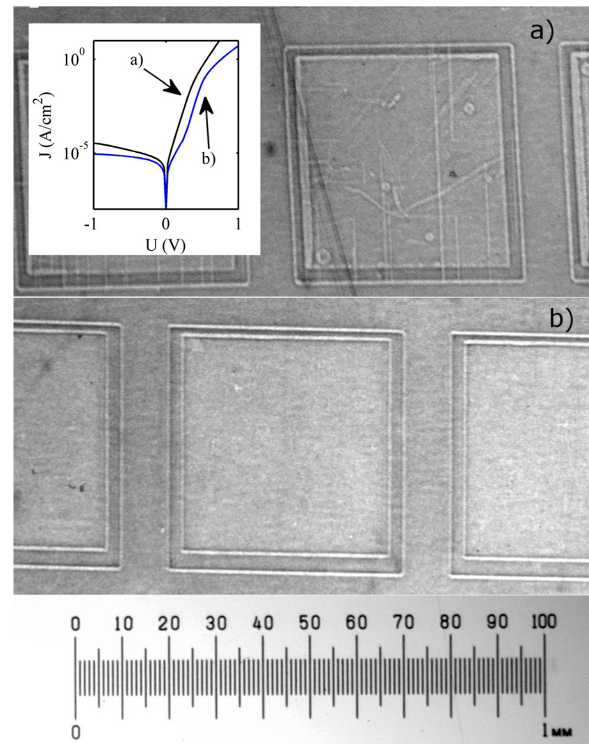

FIG. 9. 008 back-reflection XRD topographs of epitaxial structures (a) D and (b) E. The inset shows J-V curves of the corresponding mesas indicating that there is no clear correlation between crystal quality and leakage current.

suggests that the large leakages observed in some mesas are caused by defects in the epistructure dating back to the epitaxial growth process and potentially related to the pits observed in the AFM measurements.

Generally, there are several potential mechanisms and defect types that can cause leakage currents in silicon[24] but similar studies on the leakage currents of InP based materials are not available. Based on previously discussed results, however, it seems that similar reverse breakdown and local leakage current channels generated during the standard growth process of the samples are present also in standard III-V DHJ LEDs. Assuming that the leakage currents are approximately symmetric with respect to the bias voltage, the reverse leakage current can be used to approximate the additional nonradiative forward current, which reduces the

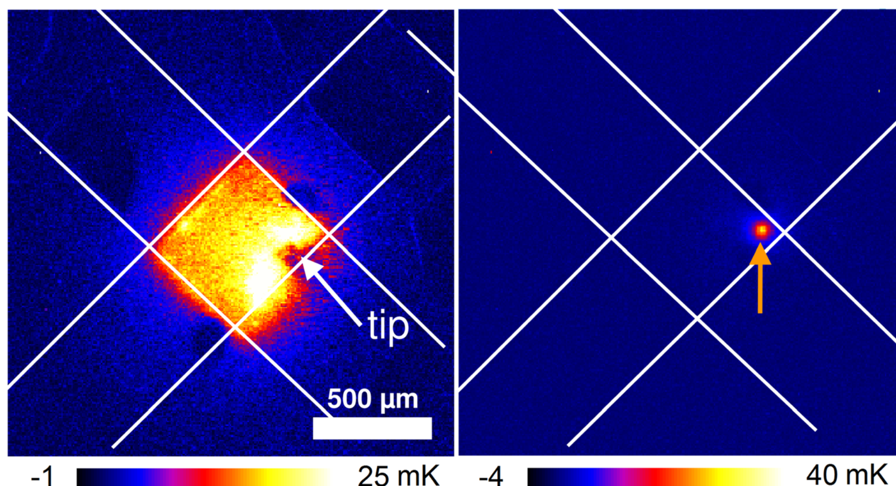

FIG. 10. DLIT amplitude signal of a leaking mesa in group D1 (a) at 0.6 V and (b) at −1 V. The white lines mark the approximate locations of the edges of the mesas and the orange arrow indicates a strong point-like heat signal under reverse bias pinpointed to be located approximately 30 μm from the edge.

[This article is copyrighted as indicated in the article. Reuse of AIP content is subject to the terms at: http://scitation.aip.org/termsconditions. Downloaded to] IP: 130.233.216.27 On: Tue, 05 May 2015 09:07:47

efficiency of the LED and prevents reaching an operating point where EL cooling is possible.

In the high power cooling regime, the quantum efficiency (EQE for conventional LEDs and a slightly modified IQE for TPX configurations) should be at least of the order of 90%–99% to allow an operating voltage that is only slightly below the voltage corresponding to the band gap of the LED. Some losses are always caused by the SRH and Auger recombinations as well as optical absorption within the structure, but it is also evident that the losses corresponding to the leakage current alone should not significantly exceed the 1% limit. One can then conclude that as long as the reverse leakage current at $-1\,\mathrm{V}$ remains at least two orders of magnitude smaller than the forward current at the typical operating point of the LED, it does not have a large effect on the LED performance apart from a potential decrease in device lifetime. However, once the surface area of the studied LEDs increases to and beyond $1\,\mathrm{cm}^2$, the probability of encountering one or more significant defects causing shunt currents larger than 1% of the radiative current increases significantly so that leakage current becomes the dominating source of nonradiative current. This presents a clear challenge for the fabrication of very high quality large area diodes using presently dominating growth conditions, and standard fabrication techniques.

IV. CONCLUSIONS

We have measured the J-V curves, leakage current statistics, and local heating distributions of a large number of double heterojunction LED structures grown at five separate facilities specialized in the growth of III-V compound semiconductors. The results suggest that there are local breakdown mechanisms that induce leakage currents that are clearly distinct from uniform nonradiative recombination or recombination at epitaxial dislocations originating from the substrates. Despite the high maturity of present fabrication and processing methods, further optimization could be needed to find conditions that optimize the performance of DHJ LED devices where the active area size is of the order of $1\,\mathrm{cm}^2$ or larger.

ACKNOWLEDGMENTS

The research has been in part supported by the Academy of Finland and the Energy efficiency program of Aalto University. The authors are grateful to T. Tuomi for the discussions relating to the XRD topography measurements.

[1]I. Schnitzer, E. Yablonovitch, C. Caneau, and T. J. Gmitter, "Ultrahigh spontaneous emission quantum efficiency, 99.7% internally and 72% externally, from AlGaAs/GaAs/AlGaAs double heterostructures," Appl. Phys. Lett. **62**(2), 131 (1993).

[2]D. A. Bender, J. G. Cederberg, C. Wang, and M. Sheik-Bahae, "Development of high quantum efficiency GaAs/GaInP double heterostructures for laser cooling," Appl. Phys. Lett. **102**(25), 252102 (2013).

[3]T. H. Gfroerer, E. A. Cornell, and M. W. Wanlass, "Efficient directional spontaneous emission from an InGaAs/InP heterostructure with an integral parabolic reflector," J. Appl. Phys. **84**(9), 5360 (1998).

[4]G. Dousmanis, C. Mueller, H. Nelson, and K. Petzinger, "Evidence of refrigerating action by means of photon emission in semiconductor diodes," Phys. Rev. **133**(1A), A316–A318 (1964).

[5]O. Heikkila, J. Oksanen, and J. Tulkki, "Ultimate limit and temperature dependency of light-emitting diode efficiency," J. Appl. Phys. **105**(9), 093119 (2009).

[6]J. Oksanen and J. Tulkki, "Thermophotonic heat pump—a theoretical model and numerical simulations," J. Appl. Phys. **107**(9), 093106 (2010).

[7]D. V. Seletskiy, S. D. Melgaard, S. Bigotta, A. Di Lieto, M. Tonelli, and M. Sheik-Bahae, "Laser cooling of solids to cryogenic temperatures," Nat. Photonics **4**(3), 161–164 (2010).

[8]M. Sheik-Bahae and R. I. Epstein, "Optical refrigeration," Nat. Photonics **1**(12), 693–699 (2007).

[9]J. Zhang, D. Li, R. Chen, and Q. Xiong, "Laser cooling of a semiconductor by 40 kelvin," Nature **493**(7433), 504–508 (2013).

[10]P. Santhanam, D. Gray, and R. Ram, "Thermoelectrically pumped light-emitting diodes operating above unity efficiency," Phys. Rev. Lett. **108**(9), 097403 (2012).

[11]D. J. Gray, P. Santhanam, and R. J. Ram, "Design for enhanced thermoelectric pumping in light emitting diodes," Appl. Phys. Lett. **103**(12), 123503 (2013).

[12]M. Konagai, M. Sugimoto, and K. Takahashi, "High efficiency GaAs thin film solar cells by peeled film technology," J. Cryst. Growth **45**, 277–280 (1978).

[13]P. Demeester, I. Pollentier, P. De Dobbelaere, C. Brys, and P. Van Daele, "Epitaxial lift-off and its applications," Semicond. Sci. Technol. **8**(6), 1124–1135 (1993).

[14]P. A. Iles, Y.-C. M. Yeh, F. H. Ho, C.-L. Chu, and C. Cheng, "High-efficiency (>20% AM0) GaAs solar cells grown on inactive-ge substrates," IEEE Electron Device Lett. **11**(4), 140–142 (1990).

[15]C. J. Keavney, V. E. Haven, and S. M. Vernon, "Emitter structures in MOCVD InP solar cells," in *Photovoltaic Specialists Conference IEEE* (1990), pp. 141–144.

[16]M. W. Wanlass, J. S. Ward, K. A. Emery, A. Duda, and T. J. Coutts, "Improved large-area, two-terminal InP/Ga0.47In0.53As tandem solar cells," in *Conference Record of the Twenty-Fourth IEEE Photovoltaic Specialists Conference* (1994), pp. 1717–1720.

[17]M. A. Green, K. Emery, Y. Hishikawa, W. Warta, and E. D. Dunlop, "Solar cell efficiency tables (version 39): Solar cell efficiency tables (version 39)," Prog. Photovoltaics **20**(1), 12–20 (2012).

[18]J. Piprek, *Semiconductor Optoelectronic Devices: Introduction to Physics and Simulation* (Academic Press, Amsterdam, 2003).

[19]E. F. Schubert, *Light-Emitting Diodes*, 2nd ed. (Cambridge University Press, Cambridge, 2006).

[20]S. Steingrube, O. Breitenstein, K. Ramspeck, S. Glunz, A. Schenk, and P. P. Altermatt, "Explanation of commonly observed shunt currents in c-si solar cells by means of recombination statistics beyond the shockley-read-hall approximation," J. Appl. Phys. **110**(1), 014515 (2011).

[21]O. Breitenstein, "Local efficiency analysis of solar cells based on lock-in thermography," Sol. Energy Mater. Sol. Cells **107**, 381–389 (2012).

[22]T. Tuomi, "Synchrotron x-ray topography of electronic materials," J. Synchrot. Radiat. **9**(3), 174–178 (2002).

[23]O. Breitenstein, *Lock-In Thermography: Basics and Use for Evaluating Electronic Devices and Materials*, Number 10 in Springer series in advanced microelectronics, 2nd ed. (Springer, Heidelberg, 2010).

[24]O. Breitenstein, J. Bauer, K. Bothe, W. Kwapil, D. Lausch, U. Rau, J. Schmidt, M. Schneemann, M. C. Schubert, J.-M. Wagner, and W. Warta, "Understanding junction breakdown in multicrystalline solar cells," J. Appl. Phys. **109**(7), 071101 (2011).

[This article is copyrighted as indicated in the article. Reuse of AIP content is subject to the terms at: http://scitation.aip.org/termsconditions. Downloaded to] IP: 130.233.216.27 On: Tue, 05 May 2015 09:07:47